Planet. Space Sci., Vol. 31, No. 3, pp. 285–293, 1983
Printed in Great Britain.

0032-0633/83/030285-09$03.00/0

EXCITATION OF AN ELECTROSTATIC WAVE BY A COLD ELECTRON CURRENT SHEET OF FINITE THICKNESS

K. S. HWANG,* ERNEST G. FONTHEIM and R. S. B. ONG*
Space Physics Research Laboratory, Department of Atmospheric and Oceanic Science,
The University of Michigan, Ann Arbor, MI 48109, U.S.A.

(*Received in final form* 18 *August* 1982)

Abstract—Electrostatic waves excited by a field-aligned electron current sheet of finite thickness are investigated. The finite width of the current sheet gives rise to boundary conditions to be satisfied at the sheet edge. This results in a restriction to the number of modes which may be driven unstable. Ducted and evanescent mode solutions are obtained. It is shown that the finite thickness of the current sheet partially stabilizes the system and contributes to the coherence of the excited waves.

INTRODUCTION

Field-aligned currents play an important role in the physics of the auroral zone. They represent part of the electrodynamic coupling between the ionosphere and the magnetosphere. At the same time, such currents often affect this coupling by exciting growing waves which, upon saturation, render the plasma turbulent. This results in anomalous electrical resistivity and the consequent field-aligned potential drops.

The subject of field-aligned currents has been reviewed by Arnoldy (1974), and Anderson and Vondrak (1975). Observations strongly indicate that upward field-aligned currents are associated with auroral displays (Arnoldy, 1974), and with plasma turbulence (Gurnett and Frank, 1973). It has also been suggested that field-aligned current driven instabilities lead to the generation of low frequency electrostatic noise in the high altitude auroral plasma (Gurnett and Frank, 1977).

The two most important current-driven instabilities in the high altitude auroral zone plasma are the ion acoustic and electrostatic ion cyclotron instabilities. One of the first investigations of the ion acoustic wave instability in an unmagnetized plasma has been carried out by Fried and Gould (1961). They showed that the critical drift velocity for instability decreases as the temperature ratio T_e/T_i increases. Drummond and Rosenbluth (1962) investigated the electrostatic ion cyclotron instability, and showed that for temperature ratios T_e/T_i near unity the critical drift velocity for instability is smaller than that for the ion acoustic instability. Kindel and Kennel (1971) extended the study of these low frequency electrostatic instabilities to a broader range of T_e/T_i and discussed both types of instabilities with reference to auroral conditions.

In all of the above treatments, the authors restricted themselves to currents or beams which are uniform and infinite in all directions, i.e., to a purely one-dimensional model. This, of course, is not correct in the applications, and it is desirable to investigate more realistic models. Recently, Elliott (1975), Dungey and Strangeway (1976) and also Strangeway (1977, 1980, 1981) have studied the electromagnetic modes of oscillation driven by a finite thickness current sheet in a plasma with a magnetic field parallel to the sheet. They showed that the instability threshold and the frequency range of unstable waves are markedly altered when the finite thickness of the current sheet is taken into account.

The object of our investigation is to determine the instability threshold and growth rates for ion acoustic and electrostatic ion cyclotron instabilities in a magnetized plasma driven by a current sheet of finite width. Some of our results have been reported earlier (Hwang *et al.*, 1979, 1981). We employ an idealized model in which the velocity distributions of the electrons and ions in the direction perpendicular to the sheet are represented by Maxwellians. Thus, the plasma has a perpendicular temperature. On the other hand, the parallel electron velocity distribution is Maxwellian outside the sheet and a delta function with a drift inside the sheet. The parallel ion distribution is a delta function everywhere. The nonzero perpendicular electron temperature allows ion-acoustic waves to propagate in the background plasma. The problem is essentially a two-dimensional one in the xz-plane. The z-axis is defined as the direction of the electron drift and the background magnetic field, while the x-axis is normal to the boundaries of the current sheet. The mathematical model is formulated in Section 2, and the

* Department of Aerospace Engineering, The University of Michigan, Ann Arbor, MI 48109, U.S.A.

basic equations are discussed. The dispersion relations are derived in Section 3 and the ducted mode solutions are discussed in Section 4.

2. FORMULATION OF THE PROBLEM

Consider the configuration as shown in Fig. 1 where the current is confined to the finite region I of half-width a, and region II represents the stationary background plasma ($|x| > a$).

Let the electrons and ions be represented by an unperturbed velocity distribution function of the form

$$f_{j0}^{(l)}(\mathbf{v}) = n_j \frac{1}{\pi v_{T_j}^2} \exp(-v_\perp^2/v_{T_j}^2)\, h_j^{(l)}(v_z) \tag{1}$$

where $l = \mathrm{I}, \mathrm{II}$, refers to the two regions in space, $j = e$, i refers to electrons and ions, v_z and $v_\perp$ are the parallel and perpendicular velocity components respectively, n_j is the number density of species j, $h_j^{(l)}$ is the parallel velocity distribution function, which is left unspecified at this time.

$v_{T_j}^2 = 2k_B T_j/m_j$
k_B = Boltzmann's constant
T_j = perpendicular temperature of species j
m_j = mass of species j

We assume quasi-neutrality, i.e., $n_e = n_i = n$. As we are interested in electrostatic waves, Maxwell's equations reduce to

$$\nabla \times \mathbf{E} = 0 \tag{2}$$

$$\nabla \cdot \mathbf{E} = 4\pi\rho \tag{3}$$

where ρ is the charge density.

The perturbations to the system are assumed to be

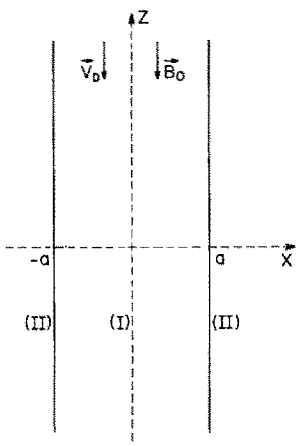

FIG. 1. TWO-DIMENSIONAL MODEL OF CURRENT SHEET OF FINITE WIDTH.

caused by electrostatic waves which are independent of y. The dispersion relation governing the behavior of these waves is obtained by evaluating the perturbation to the zero order quantities describing the system. Thus, we let

$$\tilde{f}_j^{(l)}(\mathbf{r}, \mathbf{v}, t) = f_{j0}^{(l)}(\mathbf{v}) + \varepsilon \tilde{f}_{j1}^{(l)}(\mathbf{r}, \mathbf{v}, t) \tag{4}$$

where $\tilde{f}_{j1}^{(l)}(\mathbf{r}, \mathbf{v}, t)$ is the first order distribution function and ε is a dimensionless parameter which is small compared to unity. Further,

$$\mathbf{E} = \varepsilon \tilde{\mathbf{E}}_1(\mathbf{r}, t)$$

$$\mathbf{B} = \mathbf{B}_0.$$

We assume that there is no background electric field, and that the perturbation magnetic field may be neglected as we are restricting ourselves to small amplitude electrostatic waves. Specifically, we are looking for first order quantities of the form

$$\tilde{A}_1(\mathbf{r}, t) = A_1(x)\, e^{i(\omega t - k_z z)} \tag{5}$$

where $\tilde{A}_1$ stands for either $\tilde{f}_{j1}^{(l)}$ or $\tilde{\mathbf{E}}_1$. In equation (5) the frequency is complex, i.e., $\omega = \omega_r + i\omega_i$ while k_z is assumed to be real. Thus, we are considering wave-like perturbations which are independent of y and harmonic in the z-direction. Hence, the problem is a two-dimensional one and all vectors have only components in the x and z directions. The waves above are travelling in the positive z-direction if $k_z > 0$. If the electron velocity distribution function were to have a positive slope at the phase velocity, then the waves would be amplified by the negative Landau damping. For this reason, we shall use ω and the parallel phase velocity ω/k_z as parameters describing the wave when presenting the results of the analysis.

Under the assumptions mentioned previously, the equations governing the problem are the linearized Vlasov and Maxwell equations:

$$\frac{\partial \tilde{f}_{j1}}{\partial t} + \mathbf{v} \cdot \nabla \tilde{f}_{j1} + \frac{q_j}{m_j} \frac{\mathbf{v} \times \mathbf{B}_0}{c} \cdot \nabla_{\mathbf{v}} \tilde{f}_{j1} = -\frac{q_j}{m_j} \tilde{\mathbf{E}}_1 \cdot \nabla_{\mathbf{v}} f_{j0} \tag{6}$$

$$\nabla \cdot \tilde{\mathbf{E}}_1 = 4\pi \sum_j q_j \int \tilde{f}_{j1}\, \mathrm{d}^3\mathbf{v} \tag{7}$$

$$\nabla \times \tilde{\mathbf{E}}_1 = 0. \tag{8}$$

The differential equation (6) can be solved by the method of characteristics (Krall and Trivelpiece, 1973). We introduce a set of primed variables which are defined by the unperturbed particle orbits:

$$\frac{\mathrm{d}\mathbf{r}'}{\mathrm{d}t'} = \mathbf{v}'$$

$$\frac{d\mathbf{v}'}{dt'} = \frac{q_j}{m_j}\frac{\mathbf{v}' \times \mathbf{B}_0}{c} \tag{9}$$

with the boundary conditions

$$\mathbf{r}'(t' = t) = \mathbf{r}$$
$$\mathbf{v}'(t' = t) = \mathbf{v}.$$

The solutions of equations (9) with the above boundary conditions are:

$$\begin{aligned} v'_x &= v_\perp \cos(\phi + \Omega_j \tau) \\ v'_y &= v_\perp \sin(\phi + \Omega_j \tau) \\ v'_z &= v_z \end{aligned} \tag{10}$$

and

$$\begin{aligned} x' &= x - (v_\perp/\Omega_j)[\sin(\phi + \Omega_j\tau) - \sin\phi] \\ y' &= y - (v_\perp/\Omega_j)[\cos(\phi + \Omega_j\tau) - \cos\phi] \\ z' &= z - v_z\tau \end{aligned} \tag{11}$$

where

$$\tau = t - t' \tag{12}$$

and

$$\Omega_j = q_j B_0/m_j c$$

the gyrofrequency of the jth constituent.

Expanding all functions of x' in a Taylor series about $x' = x$ yields to first order in $x' - x$

$$A(x') \approx A(x) - \frac{dA}{dx}\frac{v_\perp}{\Omega_j}[\sin(\phi + \Omega_j\tau) - \sin\phi] \tag{13}$$

where, again, A stands for either f_{j1} or $\mathbf{E}_1$. This first order approximation is valid as long as $v_\perp/\Omega_j a \ll 1$, where a is the half-width of the beam (see Fig. 1) and $v_\perp/\Omega_j \equiv r_j$ is the jth constituent Larmor radius. For a typical beam width of the order of 10 km, this inequality is usually satisfied in the top-side ionosphere (see Table 1 for the two cases treated here).

The integration over unperturbed orbits yields the following formal solution of equation (6) (Krall and Trivelpiece, 1973):

$$\tilde{f}^{(l)}_{j1} = -\frac{q_j}{m_j}\int_{-\infty}^{t} \tilde{\mathbf{E}}^{(l)}_1(\mathbf{r}', t') \cdot \nabla_{\mathbf{v}'} f^{(l)}_{j0}(\mathbf{v}')\, dt'. \tag{14}$$

From equations (1), (5), (8), (10), (11), (12), (13) and (14), the charge density becomes

$$\begin{aligned} \tilde{\rho}^{(l)}_1 &= \sum_j q_j \int \tilde{f}^{(l)}_{j1}\, d^3\mathbf{v} \\ &= \frac{1}{4\pi}\left\{\frac{\partial \tilde{E}^{(l)}_{1x}}{\partial x}\sum_j \alpha^{(l)}_{0j} - \frac{\partial \tilde{E}^{(l)}_{1z}}{\partial z}\sum_j \beta^{(l)}_j\right\} \end{aligned} \tag{15}$$

where

$$\alpha^{(l)}_{0j} \equiv \omega^2_{pj}\int_{-\infty}^{\infty} \frac{h^{(l)}_j}{(\omega - k_z v_z)^2 - \Omega_j^2}\, dv_z \tag{16}$$

$$\beta^{(l)}_j \equiv \frac{\omega^2_{pj}}{k_z}\int_{-\infty}^{\infty} \frac{\partial h^{(l)}_j/\partial v_z}{(\omega - k_z v_z)}\, dv_z \tag{17}$$

and $\omega_{pj} = (4\pi n_j q_j^2/m_j)^{1/2}$ is the plasma frequency of the jth constituent. The quantities α_{0j} contain the gyroresonance whereas the β_j contain the Landau resonance.

Combining equations (7) and (15), we obtain a wave equation of the form

$$\frac{\partial^2 E^{(l)}_{1z}}{\partial x^2} + \{k^{(l)}_x\}^2 E^{(l)}_{1z} = 0 \tag{18}$$

where

$$\{k^{(l)}_x\}^2 = k_z^2 \frac{\sum_j \beta^{(l)}_j + 1}{\sum_j \alpha^{(l)}_{0j} - 1} \tag{19}$$

is the dispersion relation for either region under consideration ($l = \mathrm{I}, \mathrm{II}$). The properties of $\{k^{(l)}_x\}^2$ determine the propagation characteristics of the wave in the x-direction. The l-dependence of $k^{(l)}_x$ refers to the region under consideration (inside or outside the current sheet). Since the parallel distribution functions $h^{(l)}_j$ are different in the two regions, the propagation characteristics are expected to be different also. In the next section the propagation characteristic for a simple model will be discussed. In addition, the boundary conditions at the sheet edge will be applied, which will result in a restriction on the number of the allowed modes. The boundary conditions will thus give rise to a set of eigenvalue equations.

TABLE 1. DERIVED PARAMETERS USED IN THIS STUDY*

Example number	Ω_i (Hz)	ω_{pi} (Hz)	Ω_e (Hz)	ω_{pe} (Hz)	V_{T_i} (cm s^{-1})	V_{T_e} (cm s^{-1})	C_s (cm s^{-1})	r_i (cm)
1	$3.05 \cdot 10^1$	$6.56 \cdot 10^3$	$5.59 \cdot 10^4$	$2.81 \cdot 10^5$	$1.06 \cdot 10^6$	$5.88 \cdot 10^7$	$1.62 \cdot 10^6$	$3.48 \cdot 10^4$
2	$1.37 \cdot 10^2$	$1.76 \cdot 10^4$	$2.52 \cdot 10^5$	$7.53 \cdot 10^5$	$1.10 \cdot 10^6$	$5.77 \cdot 10^7$	$1.24 \cdot 10^6$	$8.03 \cdot 10^3$

* Based on the model ionospheres listed in Table 2.

3. EIGENVALUE EQUATIONS

We first specify the x-dependence of the parallel distribution functions. For a first look at the effect of a current sheet of finite thickness, we chose a simple model, a cold stream of electrons inside the sheet, warm stationary electrons outside the sheet and cold stationary ions everywhere. (Note that the perpendicular velocity distributions of the electrons and ions are assumed to be Maxwellian; see equation (1).) Thus,

$$\left.\begin{aligned} h_e^{(\mathrm{I})} &= \delta(v_z - v_\mathrm{D}) \\ h_\mathrm{i}^{(\mathrm{I})} &= \delta(v_z) \end{aligned}\right\} \quad |x| < a \tag{20}$$

$$\left.\begin{aligned} h_e^{(\mathrm{II})} &= \frac{1}{\pi^{1/2} v_{T_e}} \exp(-v_z^2/v_{T_e}^2) \\ h_\mathrm{i}^{(\mathrm{II})} &= \delta(v_z) \end{aligned}\right\} \quad |x| > a \tag{21}$$

Substituting these expressions into equations (16) and (17), we can then evaluate $\{k_x^{(\mathrm{I})}\}^2$ from equation (19):

$$\{k_x^{(\mathrm{I})}\}^2 = -k_z^2 \frac{\mathrm{N(I)}}{\mathrm{D(I)}} \tag{22}$$

where

$$\mathrm{N(I)} \equiv \omega_{pe}^2/(\omega - k_z v_\mathrm{D})^2 + \omega_{pi}^2/\omega^2 - 1 \tag{23a}$$

and

$$\mathrm{D(I)} \equiv \omega_{pe}^2/[(\omega - k_z v_\mathrm{D})^2 - \Omega_e^2] + \omega_{pi}^2/(\omega^2 - \Omega_i^2) - 1 \tag{23b}$$

$$\{k_x^{(\mathrm{II})}\}^2 = -k_z^2 \frac{\mathrm{N(II)}}{\mathrm{D(II)}} \tag{24}$$

where

$$\mathrm{N(II)} \equiv (\omega_{pe}^2/k_z^2 v_{T_e}^2) Z'(\eta_e) + \omega_{pi}^2/\omega^2 - 1$$

$$\mathrm{D(II)} \equiv (\omega_{pe}^2/2k_z^2 v_{T_e}^2 \Delta_e)[Z(\eta_e + \Delta_e) - Z(\eta_e - \Delta_e)] + \omega_{pi}^2/(\omega^2 - \Omega_i^2) - 1$$

where

$$\eta_e \equiv \omega/k_z v_{T_e}$$

$$\Delta_e \equiv \Omega_e/k_z v_{T_e}$$

$$Z(\eta) \equiv \pi^{-1/2} \int_{-\infty}^{\infty} \frac{e^{-x^2}\,dx}{x - \eta} \tag{25}$$

$$Z'(\eta) = -2[1 + \eta Z(\eta)].$$

We first investigate ion-acoustic modes. In this case $\omega_r < \omega_{pi}$ and $(\omega_r/k) \leqslant c_s$ (the ion-acoustic velocity), where $k = (k_z^2 + k_x^2)^{1/2}$ if k_x is real, and $k = k_z$ if k_x is imaginary. For the wave to be unstable, the electron drift velocity must exceed the z-component of the phase velocity, while it is usually lower than the electron thermal velocity. For ion-acoustic waves it is therefore reasonable to assume that

$$\eta_e \equiv (\omega/k_z v_{T_e}) \ll 1;$$

therefore it follows that

$$Z'(\eta_e) \simeq -2$$

and for $\omega_r \ll \Omega_e$

$$Z(\eta_e + \Delta_e) - Z(\eta_e - \Delta_e) \approx 2Z_r(\Delta_e)$$

where $Z_r(\Delta_e)$ is the real part of $Z(\Delta_e)$. Hence N(II) and D(II) are approximately given by

$$\mathrm{N(II)} = (-2\omega_{pe}^2/k_z^2 v_{T_e}^2) + \omega_{pi}^2/\omega^2 - 1 \tag{26a}$$

$$\mathrm{D(II)} = (\omega_{pe}^2/k_z^2 v_{T_e}^2 \Delta_e) Z_r(\Delta_e) + \omega_{pi}^2/(\omega^2 - \Omega_i^2) - 1. \tag{26b}$$

Equations (22) and (23a, b) as well as (24) and (26a, b) are the dispersion relations for ion-acoustic waves in the finite sheet region and the background plasma, respectively. We are interested in investigating the threshold conditions for absolute instabilities. Thus, from now on, we let $\omega_i = 0$. This corresponds to the limit where there is neither Landau damping nor an instability, i.e. $\omega = \omega_r$, from which it follows that $k_x^{(I)2}/k_z^2$ is real. Hence, the ratio $k_x^{(I)2}/k_z^2$ can be either positive or negative. In the first case, $k_x^{(I)}$ is real (since k_z is taken to be real), and the solution of equation (18) yields the x-component of electrostatic waves propagating obliquely to the magnetic field with the angle of propagation determined by $k_x^{(I)}/k_z$. In the second case, $k_x^{(I)}$ is imaginary which implies an evanescent amplitude in the x-direction and electrostatic wave propagation restricted to the z-direction. This is illustrated in Figs. 2a, 2b and 2c for example 1. Table 2 lists the parameters used in this study. They were obtained from the paper by Fontheim *et al.* (1978) representing stormtime conditions at altitudes of 10,000 km (example 1) and 5000 km (example 2) respectively. Based on the above discussion, the solutions of equation (18) are therefore for $|x| < a$

$$E_{1z}^{(\mathrm{I})}(x) = \begin{cases} E_{1z0}^{(\mathrm{I})} \cos k_{xr}^{(\mathrm{I})} x & \text{if } k_x^{(\mathrm{I})} = k_{xr}^{(\mathrm{I})} \quad (27a) \\ E_{1z0}^{(\mathrm{I})} \cosh k_{xi}^{(\mathrm{I})} x & \text{if } k_x^{(\mathrm{I})} = ik_{xi}^{(\mathrm{I})} \quad (27b) \end{cases}$$

where $k_{xr}^{(\mathrm{I})}$ and $k_{xi}^{(\mathrm{I})}$ are real and for $|x| > a$

$$E_{1z}^{(\mathrm{II})}(x) = \begin{cases} E_{1z0}^{(\mathrm{II})} e^{-ik_{xr}^{(\mathrm{II})}|x|} & \text{if } k_x^{(\mathrm{II})} = k_{xr}^{(\mathrm{II})} \quad (28a) \\ E_{1z0}^{(\mathrm{II})} e^{-k_{xi}^{(\mathrm{II})}|x|} & \text{if } k_x^{(\mathrm{II})} = ik_{xi}^{(\mathrm{II})} \quad (28b) \end{cases}$$

where $k_{xr}^{(\mathrm{II})}$ and $k_{xi}^{(\mathrm{II})}$ are real. All of the above solutions are symmetrical about the plane $x = 0$ and are bounded as $|x| \to \infty$. The complete solutions for the perturbation electric field are given by (see equation (5)):

$$\tilde{E}_{1z}^{(I)}(\mathbf{r}, t) = E_{1z}^{(I)}(x)\, e^{i(\omega t - k_z z)}.$$

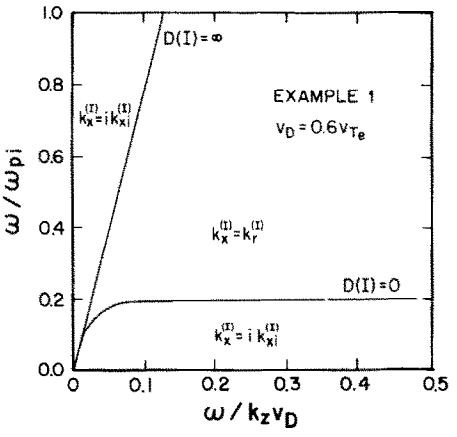

FIG. 2a. CURVES ACROSS WHICH $(k_x^{(I)})^2$ CHANGES SIGN, THUS BOUNDING THE REGIONS WHERE $k_x^{(I)} = k_{xr}^{(I)}$ AND $k_x^{(I)} = ik_{xi}^{(I)}$.

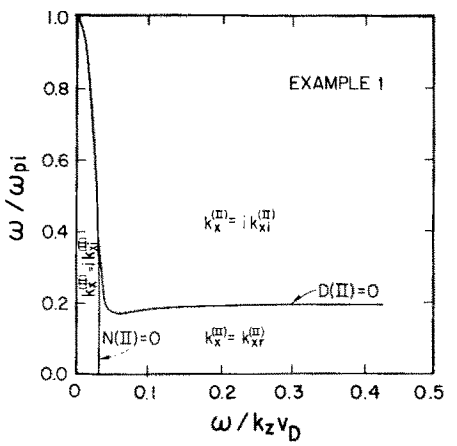

FIG. 2b. CURVES ACROSS WHICH $(k_x^{(II)})^2$ CHANGES SIGN, THUS BOUNDING THE REGIONS WHERE $k_x^{(II)} = k_{xr}^{(II)}$ AND $k_x^{(II)} = ik_{xi}^{(II)}$.

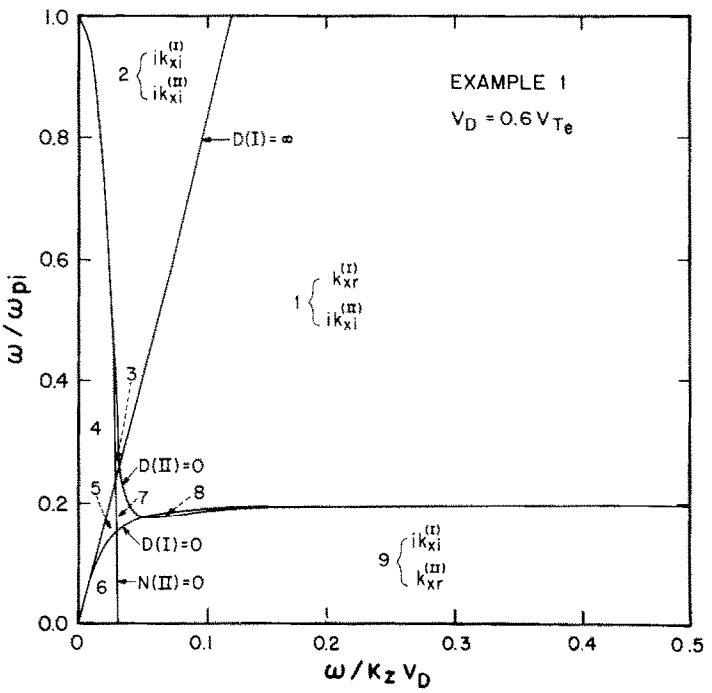

FIG. 2c. COMPLETE SET OF CURVES ACROSS WHICH EITHER $(k_x^{(I)})^2$ OR $(k_x^{(II)})^2$ CHANGES SIGN AND SHOWING THE COMBINATION OF MODES EXISTING WITHIN AND OUTSIDE OF THE CURRENT SHEET IN THE VARIOUS NUMBERED REGIONS BOUNDED BY THE CURVES.
The modes not identified on the figure are $3(ik_{xi}^{(I)}, k_{xr}^{(II)})$, $4(ik_{xi}^{(I)}, ik_{xi}^{(II)})$, $5(k_{xr}^{(I)}, ik_{xi}^{(II)})$, $6(ik_{xi}^{(I)}, ik_{xi}^{(II)})$, $7(k_{xr}^{(I)}, k_{xr}^{(II)})$, and $8(ik_{xi}^{(I)}, ik_{xi}^{(II)})$.

Inside the current sheet ($|x| < a$) the numerator of $-(k_x^{(I)}/k_z)^2$ is always positive for $\omega_r < \omega_{pi}$ (equation (23a)). For the magnetic stormtime parameters of example 1, the sign of the denominator D(I) changes across the curves D(I) = 0 and D(I) = ∞ as shown on Fig. 2a. The square of the perpendicular wave vector $k_x^{(I)}$ changes sign across these limiting curves. From

TABLE 2. MODEL IONOSPHERES USED IN THIS STUDY*

Example number	n_e (cm^{-3})	T_e (°K)	T_i (°K)	B_0 (gauss)
1	$9.8 \cdot 10^2$	$1.142 \cdot 10^4$	$6.824 \cdot 10^3$	$2.0 \cdot 10^{-2}$
2	$7.054 \cdot 10^3$	$1.097 \cdot 10^4$	$7.292 \cdot 10^3$	$9.0 \cdot 10^{-2}$

* The ions are assumed to be H^+.

equations (22) and (23b) it follows that

(a) $k_x^{(I)} = 0$ when D(I) $= \infty$,

i.e. either $(\omega - k_z v_D)^2 = \Omega_e^2$

corresponding to the Doppler-shifted electron gyro-resonance represented by the curve labelled D(I) $= \infty$ in Figs. 2a and 2c

or $\omega^2 = \Omega_i^2$

corresponding to the ion gyro-resonance not shown on the Figures because the ratio Ω_i/ω_{pi} ($\sim 5 \times 10^{-3}$) is too small, and

(b) $k_x^{(I)} = \infty$ when D(I) $= 0$,

i.e., $$\omega^2 \cong \Omega_i^2 + \frac{\omega_{pi}^2[k_z^2 v_D^2 - \Omega_e^2]}{\omega_{pe}^2 + \Omega_e^2 - k_z^2 v_D^2}.$$

In the regions where $-(k_x^{(I)}/k_z)^2 < 0$, $k_x^{(I)}$ is real, and the solution is of the form (27a). Where $-(k_x^{(I)}/k_z)^2 > 0$, $k_x^{(I)}$ is imaginary, and the solution is of the form (27b).

Outside the sheet region ($|x| > a$) both N(II) and D(II) can change sign. This is shown in Fig. 2b. These curves correspond to $k_x^{(II)} = \infty$ (when D(II) $= 0$) and $k_x^{(II)} = 0$ (when N(II) $= 0$ or D(II) $= \infty$). From equations (24), (26a) and (26b) it follows that the limiting frequencies are given by

(a) for $k_x^{(II)} = \infty$

$$\omega^2 = \frac{\omega_{pi}^2}{1 - (\omega_{pe}^2/k_z^2 v_{T_e}^2 \Delta_e) Z_r(\Delta_e)} + \Omega_i^2$$

which for $\Omega_i/\omega_{pi} \ll 1$ and $\omega_{pi}/\omega_{pe} \ll 1$ becomes

$$\omega^2 \cong \frac{\omega_{pe}^2 \Omega_e \Omega_i}{\omega_{pe}^2 + \Omega_e^2},$$

approximately the lower hybrid frequency and

(b) for $k_x^{(II)} = 0$

$$\omega^2 = k_z^2 v_{T_i}^2 \frac{T_e}{2T_i}\left(1 - \frac{\omega^2}{\omega_{pi}^2}\right)$$

or

$$\omega^2 = \Omega_i^2$$

the ion gyro-resonance. As explained above, the curve corresponding to the latter frequency is not shown on Figs 2b and c. Similarly, if $-(k_x^{(II)}/k_z)^2 < 0$, then $k_x^{(II)}$ is real, and the solution is of the form (28a). When $-(k_x^{(II)}/k_z)^2 > 0$, then $k_x^{(II)}$ is imaginary, and the solution is of the form (28b). Figure 2c shows both sets of curves, those across which $(k_x^{(I)}/k_z)^2$ changes sign and those across which $(k_x^{(II)}/k_z)^2$ changes sign. The various regions bounded by the curves define the combinations of solutions (27a, b) and (28a, b) existing in those respective regions.

The boundary conditions at the edge of the sheet ($x = \pm a$) restrict the number of permissible modes due to the finite thickness of region I. Next, the possible combinations of solutions and resulting eigenvalue relations will be discussed. The first boundary condition states that the tangential component of $\mathbf{E}_1$ must be continuous, i.e.,

$$E_{1z}^{(I)}|_{x=a-} = E_{1z}^{(II)}|_{x=a+}. \tag{29}$$

To obtain the secondary boundary condition, we combine equations (7) and (15):

$$\frac{\partial E_{1x}^{(l)}}{\partial x} + \frac{\partial E_{1z}^{(l)}}{\partial z} = \frac{\partial E_{1x}^{(l)}}{\partial x}\sum_j \alpha_{0j}^{(l)} - \frac{\partial E_{1z}^{(l)}}{\partial z}\sum_j \beta_j^{(l)}.$$

Since the coefficients $\alpha_{0j}^{(l)}$ and $\beta_j^{(l)}$ are independent of the coordinates, this can be written in the form:

$$\nabla \cdot \mathscr{F}^{(l)} = 0 \tag{30}$$

where

$$\mathscr{F}^{(l)} = \left(1 - \sum_j \alpha_{0j}^{(l)}\right) E_{1x}^{(l)} \hat{x} + \left(1 + \sum_j \beta_j^{(l)}\right) E_{1z}^{(l)} \hat{z} \tag{31}$$

If equation (30) is integrated over a volume element containing the edge of the sheet and with surfaces parallel and perpendicular to the boundary (i.e., a "pill-box"), then one obtains using Gauss' theorem:

$$\int_V \nabla \cdot \mathscr{F}\, d^3x = \oint_S \mathscr{F} \cdot \mathbf{n}\, dA = 0.$$

We let the perpendicular surfaces approach zero and obtain in the limit the second boundary condition:

$$\mathscr{F}^{(I)} \cdot \mathbf{n}|_{x=a-} = \mathscr{F}^{(II)} \cdot \mathbf{n}|_{x=a+} \tag{32}$$

or

$$\left(1 - \sum_j \alpha_{0j}^{(I)}\right) E_{1x}^{(I)}(a) = \left(1 - \sum_j \alpha_{0j}^{(II)}\right) E_{1x}^{(II)}(a).$$

From Maxwell's equation (8) and the z-dependence of the form (5) one obtains for an electrostatic wave

$$E_{1x} = \frac{i}{k_z}\frac{\partial E_{1z}}{\partial x}. \tag{33}$$

This finally leads to the second boundary condition for E_{1z}:

$$\left(1 - \sum_j \alpha_{0j}^{(I)}\right)\frac{\partial E_{1z}^{(I)}}{\partial x}\bigg|_{x=a-} = \left(1 - \sum_j \alpha_{0j}^{(II)}\right)\frac{\partial E_{1z}^{(II)}}{\partial x}\bigg|_{x=a+} \tag{34}$$

where k_z has been assumed continuous across the edge of the current sheet.

4. DUCTED MODE SOLUTIONS

Consider solutions to the wave equation (18) such that $k_x^{(I)}$ is real and $k_x^{(II)}$ is imaginary. This corresponds

to:

$$\begin{cases} E_{1z}^{(\mathrm{I})} = E_{1z0}^{(\mathrm{I})} \cos\,(k_{xr}^{(\mathrm{I})} x); & |x| < a \\ E_{1z}^{(\mathrm{II})} = E_{1z0}^{(\mathrm{II})} \exp\,(-k_{xi}^{(\mathrm{II})}|x|); & |x| > a \end{cases} \tag{35}$$

where $k_x^{(\mathrm{I})} = k_{xr}^{(\mathrm{I})}$ and $k_x^{(\mathrm{II})} = ik_{xi}^{(\mathrm{II})}$. Inside the sheet this pair of solutions corresponds to a standing wave pattern in the transverse direction propagating in the parallel direction, while outside the sheet the amplitude falls off exponentially with distance away from the sheet. This pair of solutions is therefore called by us the ducted wave mode. These solutions are lying in regions 1 and 5 of Fig. 2c.

We notice that in region 1 of Fig. 2c the waves are located between the Doppler-shifted electron gyrofrequency and the lower hybrid frequency. Applying the boundary conditions (29) and (34) yields at $x = a$:

$$E_{1z0}^{(\mathrm{I})} \cos\,(k_{xr}^{(\mathrm{I})} a) = E_{1z0}^{(\mathrm{II})} \exp(-k_{xi}^{(\mathrm{II})} a)$$

$$\left(1 - \sum_j \alpha_{0j}^{(\mathrm{I})}\right) k_{xr}^{(\mathrm{I})} E_{1z0}^{(\mathrm{I})} \sin\,(k_{xr}^{(\mathrm{I})} a)$$

$$= \left(1 - \sum_j \alpha_{0j}^{(\mathrm{II})}\right) k_{xi}^{(\mathrm{II})} \cdot E_{1z0}^{(\mathrm{II})} \exp\,(-k_{xi}^{(\mathrm{II})} a).$$

We divide these two equations by each other and use the definitions of $k_{xi}^{(\mathrm{II})}$ and $k_{xr}^{(\mathrm{I})}$. The result is the following eigenvalue relation:

$$(1-\alpha_{0e}^{(\mathrm{I})}-\alpha_{0i}^{(\mathrm{I})})^{1/2}(-\beta_e^{(\mathrm{I})}-\beta_i^{(\mathrm{I})}-1)^{1/2} \tan\,(k_{xr}^{(\mathrm{I})} a)$$
$$= (1-\alpha_{0e}^{(\mathrm{II})}-\alpha_{0i}^{(\mathrm{II})})^{1/2}(1+\beta_e^{(\mathrm{II})}+\beta_i^{(\mathrm{II})})^{1/2}. \tag{36}$$

The functions $\alpha_{0j}^{(\mathrm{I})}$ and $\beta_j^{(\mathrm{I})}$ are defined in equations (16) and (17), with the parallel distribution functions $h_j^{(\mathrm{I})}$ given by expressions (20) and (21). Hence, equation (36) gives the relation between the wave parameters ω, $k_{xr}^{(\mathrm{I})}$ and k_z on the one hand and the parameters of the two plasma regions on the other. The latter are the electron drift and thermal velocities (v_{D}, v_{T_e}), the electron and ion gyrofrequencies (Ω_e, Ω_i), the electron and ion plasma frequencies (ω_{pe}, ω_{pi}), and the sheet half-width a. Equation (36) is not a dispersion relation as is evident from the fact that it depends on the properties of both plasma regions. Rather it restricts the possible modes ($\omega, k_{xr}^{(\mathrm{I})}, k_z$) which can exist at threshold conditions in a current sheet embedded in a background plasma. Such a separate condition defining the allowable modes based on boundary conditions is commonly referred to as an eigenvalue equation.

Restricting ourselves to real values of ω, we thus obtain the marginal stability curves for the ducted modes. These are shown in Fig. 3 for example 1. For any particular value of the sheet half-width a, the region below and to the right of the curve indicates values of ω_r/k_z and complex ω with $\omega_i < 0$ satisfying the relation (36). Thus, in this region negative Landau damping may

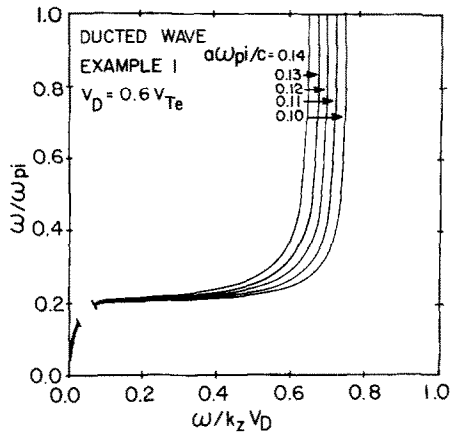

FIG. 3. EIGENVALUE SOLUTIONS OF THE DUCTED WAVE FOR EXAMPLE 1 WITH THE CURRENT HALF-WIDTH AS A PARAMETER. The gap in these curves and in those of Figs. 4–7 represents the jump across region 7 of Fig. 2c associated with refracted modes.

lead to instabilities, excited by the electron drift current. The region of instability extends to the right of each marginal curve up to at most the line $\omega/k_z v_{\mathrm{D}} = 1$. Hence, we can see from Fig. 3 that, with v_{D} fixed, a thick current sheet is more unstable than a thin one. We can also fix the sheet half-width a and obtain the relation between ω/k_z and ω with the electron drift current v_{D} as a parameter. These are shown in Fig. 4 again for example 1. Just as in Fig. 3, the instability region for a given drift velocity is located between the corresponding threshold curve and the line $\omega/k_z v_{\mathrm{D}} = 1$. Since the normalization of the phase velocity ω/k_z is with respect to the drift velocity v_{D}, each of the curves of Figs. 4 and 6 is normalized to its own value of v_{D}. The respective sizes of the instability regions for various drift velocities can

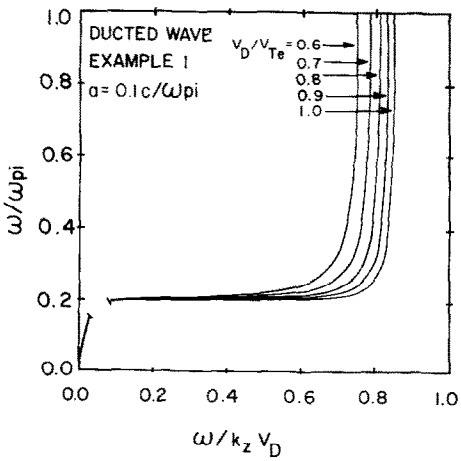

FIG. 4. EIGENVALUE SOLUTIONS OF THE DUCTED WAVE FOR EXAMPLE 1 WITH THE DRIFT VELOCITY v_{D} AS A PARAMETER.

therefore not be compared directly in those two figures. It can be shown, however, that the number of potentially unstable modes slightly increases with increasing v_D.

Similar curves for the parameters of example 2 are shown in Figs. 5 and 6. The ducted mode curves in Figs. 3–6 originate in the narrow wedge-shaped region 5 of Fig. 2c at the origin and continue up to the boundary curve N(II) = 0. They are discontinuous across region 7 which is associated with refracted wave modes (propagating waves both inside and outside the current sheet) with frequencies of the order of $\omega/\omega_{pi} \sim 0.2$ and then continue in region 1 of Fig. 2c. The refracted modes will be discussed in a separate paper.

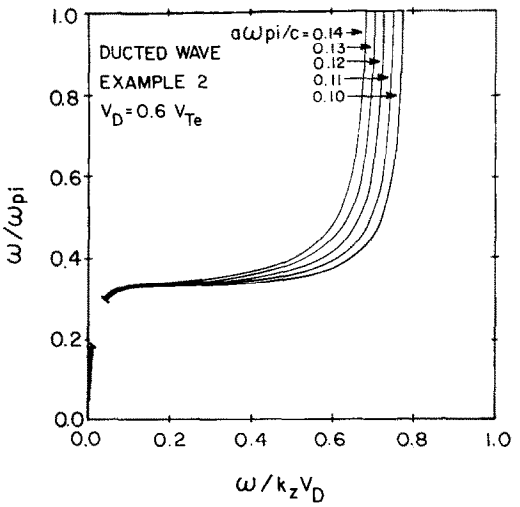

FIG. 5. EIGENVALUE SOLUTIONS OF THE DUCTED WAVE FOR EXAMPLE 2 WITH THE CURRENT HALF-WIDTH AS A PARAMETER.

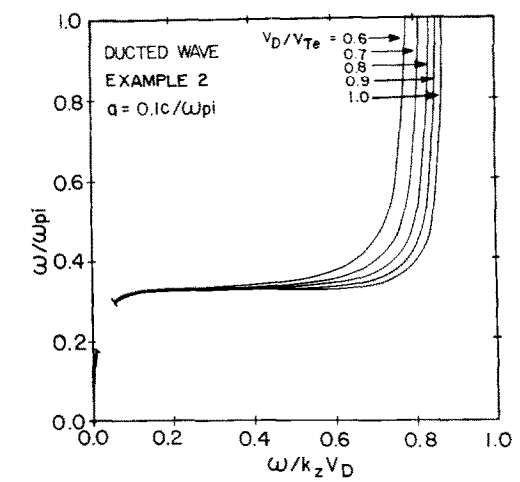

FIG. 6. EIGENVALUE SOLUTIONS OF THE DUCTED WAVE FOR EXAMPLE 2 WITH THE DRIFT VELOCITY v_D AS A PARAMETER.

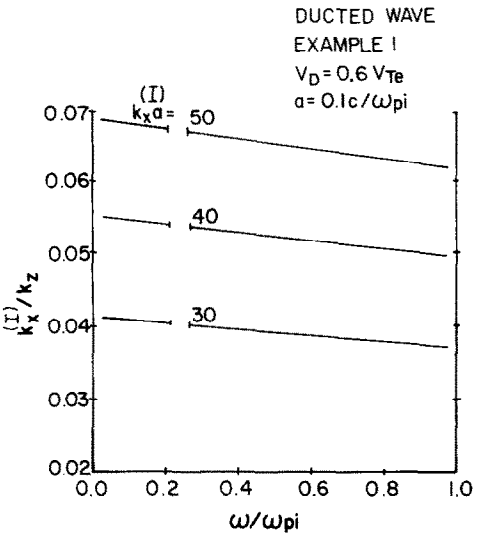

FIG. 7. THE MAGNITUDE OF $k_x^{(I)}/k_z$ VS ω/ω_{pi} OF THE DUCTED WAVE AT VARIOUS $k_x^{(I)}a$ FOR EXAMPLE 1.

We note that in region (I), i.e., inside the current sheet, both $k_x^{(I)}$ and k_z are real. This means that the waves are propagating in a direction oblique to the background magnetic field. The ratio $k_x^{(I)}/k_z$ for a wave with $k_x^{(I)}a \simeq 50$ is shown in Fig. 7 as a function of ω/ω_{pi}. It is to be observed that $k_x^{(I)}$, although non-zero, is very small compared with k_z. Thus, the waves propagate in a direction almost parallel with the background magnetic field. As $k_x^{(I)}/k_z = E_{1x}/E_{1z}$, we also see that the transverse wave electric field E_{1x} is much smaller than the longitudinal component E_{1z}. Figure 7 shows similar results for the cases where $k_x^{(I)}a \approx 40$ and 30. One can see from these curves that $k_x^{(I)}/k_z$ decreases as $k_x^{(I)}a$ decreases. This confirms that for a fixed beam width the electric field becomes more field-aligned as the wavelength increases, which is a property of electrostatic waves. It also shows that for fixed wavelength the electric field becomes more field-aligned as the beam width decreases. As explained above, the discontinuity in each curve represents the jump across region 7 of Fig. 2c.

5. DISCUSSION

By means of a simple model we have studied the excitation of ion-acoustic instabilities by a finite thickness cold electron current sheet in a plasma with a background magnetic field directed parallel to the sheet. The electron and ion distribution functions in the plane perpendicular to the magnetic field are taken to be Maxwellian. The parallel ion distribution is a delta function with zero drift everywhere, and the parallel electron distribution is a delta function with drift

velocity v_D inside the sheet and with zero drift outside the sheet. As the parallel ion distribution inside the sheet is assumed to be a delta function, ion Landau damping is not taken into account. The boundaries of the current sheet are assumed to be sharp. This is reasonable as the typical thickness of the electron current sheet in the high altitude auroral zone (10–30 km) is much larger than the corresponding ion Larmor radius (see Table 1).

The threshold conditions for ion acoustic instabilities have been carefully examined. The main results of the analysis are summarized by the various regions in Fig. 2c. Regions 1 and 5 yield ducted mode solutions. In this case only ion-acoustic waves can be excited as the frequency range in these regions far exceeds the ion cyclotron frequency ($\Omega_i \ll \omega < \omega_{pi}$). These waves propagate in a direction almost parallel to the background magnetic field. For a constant electron drift velocity, a thick current sheet is found to be more unstable than a thin one. Moreover, fewer modes can turn unstable as the current sheet thickness is reduced. Thus, the finite thickness of the electron current sheet contributes to the coherence of the excited waves.

The regions 2, 4, 6 and 8 of Fig. 2c correspond to evanescent modes. These are ion-acoustic waves propagating parallel to the background magnetic field. The wave amplitude of these waves increases perpendicular to B_0 inside the current sheet and decreases outside the sheet.

Regions 3, 7 and 9 are very similar; they correspond to the situation where the excited mode has a periodic solution outside the current sheet ($k_x^{(II)}$ is real). Thus, in this case, the cold electron current excites radiating modes which propagate in the background plasma outside the sheet. In region 9 of Fig. 2c not only ion-acoustic waves, but also electrostatic ion cyclotron waves with frequencies in the neighbourhood of the ion cyclotron frequency can be excited.

In conclusion, we find that the finite thickness of the electron current sheet partially stabilizes the system in regard to the excitation of electrostatic waves. It is more difficult to excite electrostatic waves as the thickness of the current sheet is decreased. Also the range in wave frequencies and phase velocities of the unstable waves are reduced. This indicates that the finite thickness of the electron current sheet tends to make the excited electrostatic waves more coherent.

Acknowledgements—The authors thank R. J. Strangeway for a number of stimulating discussions and good suggestions. This research was supported by the Atmospheric Sciences Section of the National Science Foundation through grant ATM-8015810 and by the National Aeronautics and Space Administration through grant NGR23-005-015.

REFERENCES

Anderson, H. K. and Vondrak, R. R. (1975) Observations of Birkeland currents at auroral latitudes. *Rev. Geophys. Space Phys.* **13**, 243.

Arnoldy, R. L. (1974) Auroral particle precipitation and Birkeland currents. *Rev. Geophys. Space Phys.* **12**, 217.

Drummond, W. E. and Rosenbluth, M. N. (1962) Anomalous diffusion arising from micro-instabilities in a plasma. *Physics Fluids* **5**, 1507.

Dungey, J. W. and Strangeway, R. J. (1976) Instability of a thin field-aligned electron beam in a plasma. *Planet. Space Sci.* **24**, 731.

Elliott, D. T. (1975) The ducting of wave energy by field-aligned current sheets. *Planet. Space Sci.* **23**, 751.

Fontheim, E. G., Ong, R. S. B., Roble, R. G., Mayr, H. G., Baron, M. J., Hoegy, W. H., Wickwar, V. B., Vondrak, R. R. and Ionson, J. A. (1978) Effect of anomalous transport coefficients on the thermal structure of the storm-time auroral ionosphere. *J. geophys. Res.* **83**, 4831.

Fried, B. D. and Gould, K. W. (1961) Longitudinal ion oscillations in a hot plasma. *Physics Fluids* **4**, 139.

Gurnett, D. A. (1974) The earth as a radio source: Terrestrial kilometric radiation. *J. geophys. Res.* **79**, 4227.

Gurnett, D. A. and Frank, L. A. (1973) Observed relationships between electric fields and auroral particle precipitation. *J. geophys. Res.* **78**, 145.

Gurnett, D. A. and Frank, L. A. (1977) A region of intense plasma wave turbulence on auroral field lines. *J. geophys. Res.* **82**, 1031.

Hwang, K.-S., Ong, R. S. B. and Fontheim, E. G. (1979) Ion-acoustic wave instability excited by a current sheet of finite width in the auroral zone. *Trans. Am. geophys. Un.* **60**, 914.

Hwang, K.-S., Ong, R. S. B. and Fontheim, E. G. (1981) Instability thresholds and electrostatic wave emission by two models of field-aligned current sheets. *Trans. Am. geophys. Un.* **62**, 352.

Kindel, J. M. and Kennel, C. F. (1971) Topside current instabilities. *J. geophys. Res.* **76**, 3055.

Krall, N. A. and Trivelpiece, A. W. (1973) *Principles of Plasma Physics*, Section 8.8. McGraw-Hill, New York.

Strangeway, R. J. (1977) Further results from a model for a thin field-aligned electron beam in a plasma. *Planet. Space Sci.* **25**, 795.

Strangeway, R. J. (1980) On the instability of a spatially continued electron beam in a magnetized plasma. *J. Plasma Phys.* **24**: 2, 193.

Strangeway, R. J. (1981) The significance of temperature in a finite geometry electron beam-plasma system. *J. geophys. Res.* **86**, 9079.